Volume 9
Number 2
February 2024
Pages 213–486

Reaction Chemistry & Engineering

Linking fundamental chemistry and engineering to create scalable, efficient processes

rsc.li/reaction-engineering

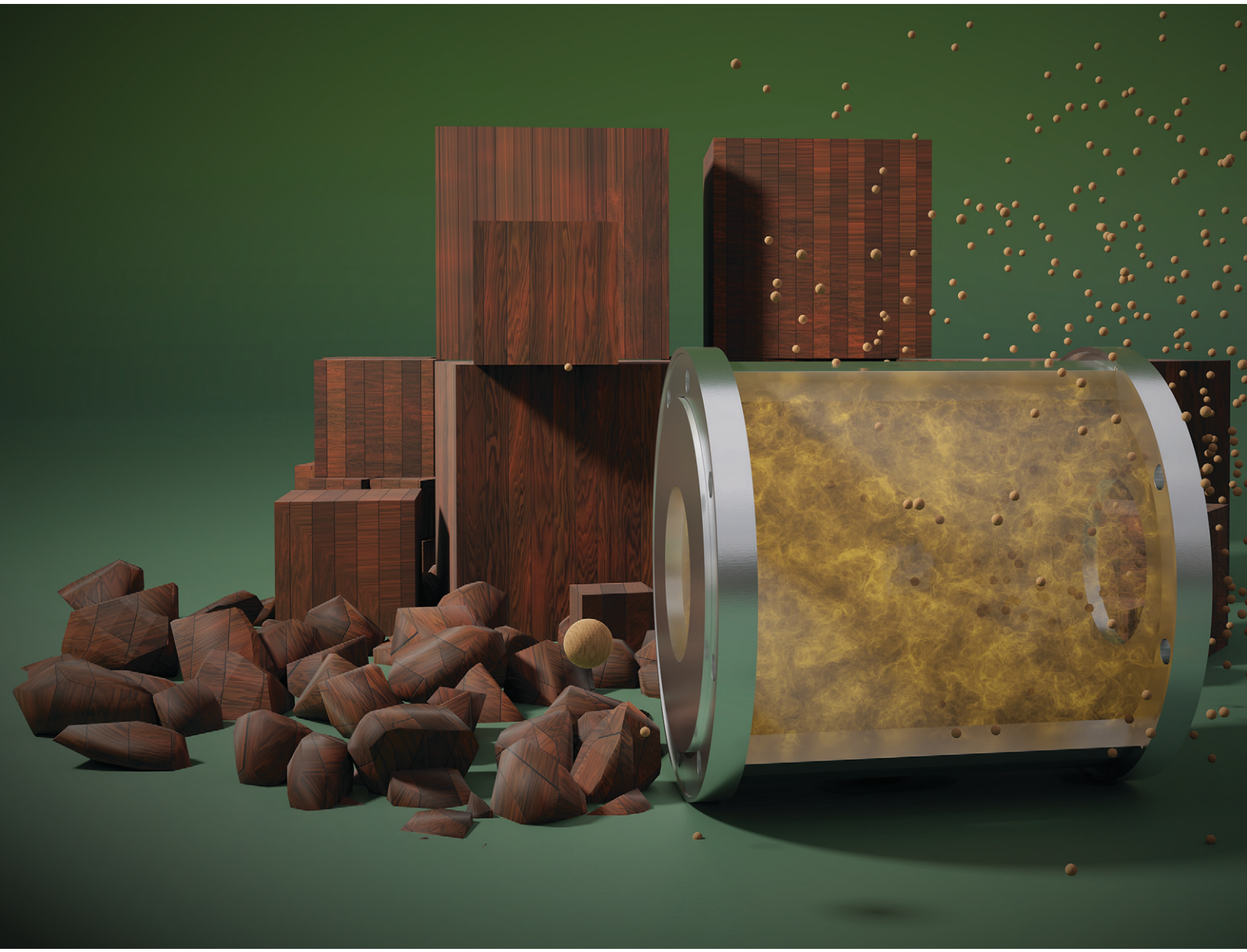

ISSN 2058-9883

ROYAL SOCIETY OF CHEMISTRY

PAPER

E. Johan Foster *et al.*

Binary mixture of subcritical water and acetone: a hybrid solvent system towards the production of lignin nanoparticles

Reaction Chemistry & Engineering

ROYAL SOCIETY OF CHEMISTRY

PAPER

View Article Online
View Journal | View Issue

Cite this: *React. Chem. Eng.*, 2024, **9**, 226

Binary mixture of subcritical water and acetone: a hybrid solvent system towards the production of lignin nanoparticles†

Philip S. McMichael,[ab] Mahfuzul Hoque,[ab] Fernanda Brito dos Santos,[ab] Victoria French[ab] and E. Johan Foster *[ab]

Received 8th August 2023,
Accepted 6th November 2023

DOI: 10.1039/d3re00424d

rsc.li/reaction-engineering

Valorization of technical lignin is crucial for the circular bioeconomy – this can be achieved by the transformation of lignin to high-value nanomaterials. However, the majority of lignin nanoparticle (LNP) production methods require high volumes of organic solvent, and specialized equipment, or fail in certain cases to produce a morphologically uniform product with superior physicochemical properties to technical lignin. Herein, a binary solvent system of subcritical water and acetone based on the principles of solvent–antisolvent (SAS) precipitation of lignin is proposed. Spherical LNPs with a high degree of uniformity in the chemical structure are produced *via* a batch reactor from kraft lignin demonstrating high yield (88–92%), colloidal stability in water, thermal stability, and low mean particle size – these are desirable for advanced biocomposite and biomedical applications; achieved in this study by using lower volumes of recyclable acetone (4–7 times less) than previously reported.

Introduction

Chemical industries are the third largest producers of global carbon dioxide emissions owing to their reliance on fossil fuels derived feedstocks, necessitating their reinvention *via* innovative reaction engineering solutions. Fueled by the global climate change crisis (global warming), and the acute health concerns stemming from petroleum-derived plastics,[1] there has been an upsurge in preference for renewable and "earth-friendly" materials and products.

One such renewable chemical is lignin, an aromatic biopolymer found in the cell walls of all vascular plants, which is produced in large quantities worldwide[2] and comprises 20–30% of the total mass of most commercial tree species.[3] The pulp and paper industry are the chief producers of purified lignin, which is primarily extracted from the by-product (black liquor) of the pulping processes including kraft pulping. Industrial lignin makes up 35–45% of the solids content of black liquor and can be extracted through a variety of established methods (kraft, organosolv, and lignosulfonate, to name a few) resulting in amorphous lignin with different structural features (*i.e.*, formation of recalcitrant C–C bonds) to that of native lignin, hence, it is called technical lignin. Now, although nearly 70 million tons of kraft lignin (a type of softwood-derived technical lignin) is produced annually,[4,5] over 98% is burned for energy recovery in pulp and paper mills[6] – an opportunity for chemical reaction engineering and process development to change the paradigm of lignin valorization.

Interestingly, the production of LNPs has emerged as a means of improving the morphological and chemical uniformity of lignin – owing to an increased surface area to volume ratio, they can demonstrate unique properties, including improved UV protection, antibacterial, and anti-oxidant properties.[7,8] Also, this leads to higher reactivity (of phenolic and aliphatic hydroxyl groups[9]), which affords the development of advanced functional materials, including CO_2/N_2-switchable Pickering emulsions.[10] Furthermore, improved miscibility in water as well as in polymers (*i.e.*, high-density polyethylene[11]) broadens the application portfolio of lignin, as a drug carrier (*i.e.*, curcumirin[12]), for adhesives,[13] composites,[14] and coatings.[15]

The reaction chemistry to produce LNPs involves predominantly wet chemistry and hydrodynamics-based approaches, which includes pH and solvent shifting, antisolvent precipitation, polymerization (*e.g.*, graft) and spray drying, electrospinning, self-assembly and more.[16,17] Details about these methods can be found elsewhere.[18] Now, most methods suffer from various drawbacks, including dependence on high volumes of organic solvents, low process yields, multi-step procedures, and expensive equipment designed for laboratory environments.[19]

[a] *Department of Chemical and Biological Engineering, University of British Columbia, 2385 East Mall, Pulp and Paper Centre, V6T 1Z4, Canada. E-mail: johan.foster@ubc.ca*
[b] *Bioproducts Institute, 2385 East Mall Vancouver, BC, V6T 1Z4, Canada*

† Electronic supplementary information (ESI) available: Additional AFM images, CHNS Elemental Analysis of samples, Fourier-transform infrared spectroscopy and accompanying discussion, 7 pages. See DOI: https://doi.org/10.1039/d3re00424d

In this work, we present a process for the synthesis of LNPs using a novel system that relies on the solvent–antisolvent (SAS) method combined with the inherent properties of water at subcritical conditions (Fig. 1). The term scH_2O refers to water above its atmospheric pressure boiling point of 100 °C, at elevated pressure to maintain its liquid phase, but at conditions below its critical point (374 °C with a vapor pressure of 22 MPa).[20] At subcritical conditions, water can reach a relative permittivity (dielectric constant) near that of common organic solvents like dimethyl sulfoxide, methanol, and acetone. ScH_2O functions as a solvent for certain organic non-polar compounds, including lignin, effective for hydrolysis and fractionation and production of bio-oils from lignocellulosic biomasses.[21–24] However, no present work has demonstrated its use to produce LNPs from technical lignin.

We note that the SAS precipitation method to produce nanoparticles has been utilized for a range of nanoparticle suspensions, including to produce germanium and silver nanoparticles,[27] semiconductor nanoparticles,[28] and nanopharmaceutical applications.[29,30] *Via* SAS, production of LNPs works by mixing dry lignin powder with a solvent (most commonly tetrahydrofuran or acetone, though ethylene glycol,[13] ethanol,[31] γ-valerolactone,[32] and other solvents have been used), which provides a completely solubilized lignin solution, followed by mixing with an antisolvent; a chemical (commonly water for kraft lignin) that lignin is completely insoluble in. Thus, owing to the increase in the chemical potential (caused by the antisolvent), the rapid supersaturation leads to spontaneous homogenous nucleation of particles (crystalline/amorphous),[33] forming stable colloidal suspensions in the resultant SAS mixture. This self-assembly process driven by solvent–solvent interactions ensure uniform spherical morphology of the amorphous LNPs. However, large volumes of organic solvents are needed to produce relatively low amounts of LNPs.[16,19,34]

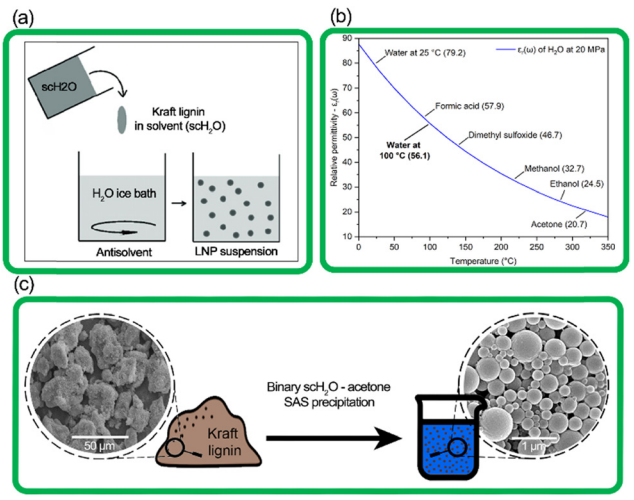

Fig. 1 (a) The simplified process of SAS precipitation of nanoparticles,[25] (b) the relative permittivity ($\varepsilon_r(\omega)$) of water at increasing temperature, with constant pressure of 20 MPa, and $\varepsilon_r(\omega)$ of common solvents for reference (Uematsu *et al.* 1980),[26] (c) transition from amorphous kraft lignin to spherical lignin nanoparticles, as seen by SEM images.

In this study, scH_2O was rapidly expelled from the high-pressure reactor and rapidly mixed with water below room temperature, in the form of an ice bath, to ensure that spontaneous nucleation of new nanoparticles was favored over growth of particle aggregates, according to prior literature which suggests a clear correlation between faster SAS mixing rates and smaller mean particle diameter.[35,36] This hybrid scH_2O is assisted by low volumes of recyclable acetone (several orders lower than previously reported), effectively solubilizing lignin to produce chemically and morphologically uniform LNPs, and the synthesized LNPs were investigated for morphological, chemical, and particle size uniformity, as well as thermal and colloidal stability.

Methods

Materials

Kraft lignin produced through the LignoBoost® process, from a chip furnish of 30% interior (white/Engelmann) spruce, 60% lodgepole pine, and 10% subalpine fir was provided by Canfor Corporation (Vancouver, BC, Canada). Reagent-grade acetone (>99% purity) was purchased from Sigma-Aldrich (St. Louis, MO, USA). A 500 mL volume high-pressure/high-temperature batch reactor, model 4575 from Parr Instrument Company (Moline, IL, USA) was used, and pressurized with N_2 gas (99.999% purity) from Airgas, Inc. (Radnor, PA, USA).

Production of LNPs

Kraft lignin on a dry weight basis was weighted out based on a concentration of 5 grams per liter and added to solutions of acetone (based on a volume by total volume percentage) and completed with water to a total volume of 250 mL. Three samples of 5 g L^{-1} kraft lignin were prepared, 2.5% acetone with 97.5% deionized (DI, Milli-Q®) H_2O (labeled 2.5%A LNPs), 5% acetone with 95% DI H_2O (labeled 5%A LNPs), and 10% acetone with 90% DI H_2O (labeled 10%A LNPs). An additional sample of 5 g L^{-1} kraft lignin in 250 mL of DI H_2O, without acetone, was prepared (labeled 0%A lignin). Each sample was then stirred using an IKA (Staufen, DE) T-25 Ultra-Turrax homogenizer for 5 minutes at 10 000 rpm. A 50 mL aliquot of each sample was then taken and stored for further characterization and comparison.

Each 200 mL sample was then placed in the Parr 4575 reactor, which was then sealed and pressurized to 15 MPa with N_2 gas. A heating rate of 2.5 °C per minute was used to heat the samples from 25 °C to 100 °C, which raised internal reactor pressure to 20 MPa. Due to the higher vapor pressure of acetone than water, samples with higher concentrations of acetone had slightly higher pressures at 100 °C. After heating, the pressure of these samples was decreased to 20 MPa, using a gas outlet valve, to ensure a standard pressure for all tests. Samples were held at 100 °C and 20 MPa for 1 hour, with continuous stirring at 200 rpm. After 1 hour, the sample outlet valve was opened and the solution was rapidly expelled from the reactor into 400

mL of DI water mixed with crushed ice, allowing for rapid mixing of the solvent and anti-solvent. Each acetone-containing sample then underwent rotary evaporation at 65 °C for two hours, to ensure total removal of acetone. 200 mL of each sample was then set aside to be frozen for lyophilization, while the remaining sample was stored in solution at 4 °C. Fig. 2 outlines the LNP production using the high-pressure reactor.

Analytical methods

Lignin samples for morphological analysis with scanning electron microscopy (SEM) (Helios NanoLab 650, FEI, Hillsboro, OR, USA) were prepared using a 0.1 wt% and 0.01 wt% dilution of prepared LNPs in DI water. Carbon tape was placed on SEM pin stubs, and 100 μL of the diluted LNP solution was pipetted onto the surface of the tape and dried at 60 °C until excess water was evaporated. The procedure of pipetting and drying was repeated three times, to ensure that enough LNP sample was present on the SEM stub. ImageJ image processing software was used to analyze SEM images and estimate particle size based on SEM imagery, with a sample size of 200 particles for each particle size distribution histogram generated. The particle size distribution of lignin particles was also studied by use of a laser diffraction particle size analyzer (Mastersizer 3000, Malvern Panalytical, UK). Span values of particle size distribution were calculated by eqn (1), with D_{90}, D_{50}, and D_{10} being the points in the size distribution that 90%, 50% and 10% of total material volume is contained within (smaller than), respectively.

$$\text{Span} = \frac{D_{90} - D_{10}}{D_{50}} \quad (1)$$

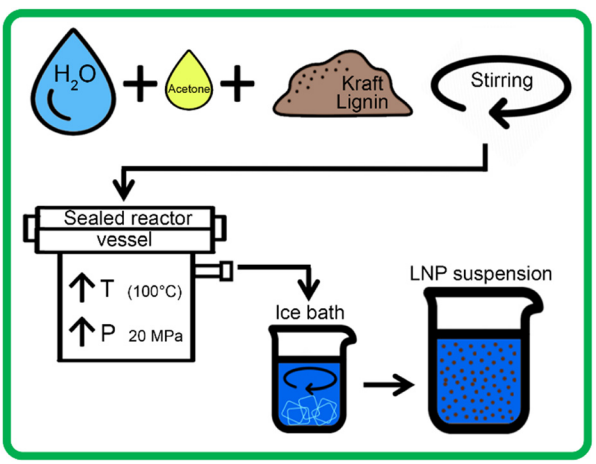

Fig. 2 Illustration of process of synthesizing LNPs using SAS process with scH_2O and acetone, showing general conditions in high pressure reactor, followed by rapid mixing with ice bath, to generate colloidally stable LNP suspension, to be followed by rotary evaporation. The size of the droplets (top-left side) corresponding to water (blue-colored) and the acetone (yellow-colored) signify the relative proportion of the volume used to produce LNPs.

Table 1 Sample yield was calculated based on weight of sample extracted from reactor, and T_{onset} was calculated following ISO 11358-1. Decreased in-reactor aggregation and smaller particle size led to a higher recoverable yield of LNPs

Sample name	Yield	T_{onset} (°C)	Span	Zeta potential (mV)
0%A lignin	71%	240	127.8	−20.7 ± 1.7
2.5%A LNPs	88%	226	11.4	−37.5 ± 4.9
5%A LNPs	91%	283	25.4	−50.3 ± 2.3
10%A LNPs	92%	292	1.6	−52.6 ± 0.8

The undiluted liquid sample was sonicated at 80% amplitude for 60 seconds using the built-in equipment sonicator and measured at a set obscuration of 5%. Thermal degradation of lyophilized lignin samples was analyzed with thermogravimetric analysis (TGA) equipment (TGA 5500, TA Instruments, USA), using a heating ramp rate of 10 °C per minute, up to 800 °C. OriginPro Software (2022 Version, OriginLab, USA) was used to analyze the derivative thermogravimetry (DTG) of the samples. The onset temperature of thermal degradation, shown in Table 1, was calculated according to procedures outlined in ISO 11358-1. Sample yield was calculated based on the total dry weight of the sample extracted after lyophilization, as a fraction of the initial dry weight of the kraft lignin sample mixed with acetone/water solutions, given a lignin concentration of 5 grams per liter. Zeta potential analysis was conducted with Malvern Zetasizer Nano DLS equipment (Malvern Panalytical, UK), with sample concentrations in DI water set at 0.01 g L^{-1} for all measurements. Hansen solubility parameters and spheres were calculated with assistance of the HSP Excel Spreadsheet provided by **https://www.hansen-solubility.com**. Lignin was mixed at a concentration of 0.5 g L^{-1} in 20 common solvents, (coordinates given in Fig. S5†) stirred overnight, and allowed to settle for 24 hours before solubility assessments were made.

Results and discussion

Uniform LNP synthesis with scH_2O and acetone treatment

To maximize the yield of LNPs (>90%), total lignin de-aggregation, followed by complete solubilization, is necessary. As such, a variety of reactor conditions were initially evaluated to determine optimal conditions for LNP synthesis. At temperatures at and above 250 °C, the burning of lignin was evident in the reactor system, while at temperatures above 150 °C, thermal degradation of the lignin was still evident (confirmed through TGA) with increased aggregation of lignin particles in the reactor. A temperature of 100 °C was found to be sufficient for LNP synthesis while limiting thermal degradation and particle aggregation in the reactor. At this temperature, a pressure greater than 0.364 MPa (3.58 atm) is necessary to maintain acetone/water solutions in a purely liquid phase, given the vapor pressure of acetone at 100 °C. However, reactions at higher pressures were found to be more effective at decreasing particle size,

compared with reactions at pressures only slightly above 0.364 MPa. The effect of pressure has been previously found to have a negligible effect on the solubilities of most organic compounds in scH_2O.[37] There exists the possibility that high pressure may aid this unique process of nanoparticle synthesis in several ways, including preventing aggregation of subcritical-water-insoluble portions of lignin, which may function as nucleation sites during the SAS precipitation step, and in turn may encourage excessively large sphere growth, rather than new sphere formation.

Additionally, higher reactor pressures translated to more rapid and complete expulsion of the sample from the high-pressure reactor into the ice bath, allowing for a greater portion of the sample to undergo SAS nucleation. Faster rates of solvent and antisolvent mixing have been shown to directly correlate to smaller particle sizes, due to high supersaturation favoring new sphere formation. If an environment of high supersaturation can be quickly achieved, the unfavorable growth of existing spheres, rather than nucleation of new spheres, can be avoided.[38–40] Exploratory tests found that a reactor pressure of 20 MPa was found to produce a higher yield of nanoparticles compared with pressures of 15 MPa and 10 MPa. After the temperature ramp-up, all samples were held at 20 MPa and 100 °C for 60 minutes. Preliminary tests showed that increasing holding time from 60 minutes to 120 and 180 minutes had negligible effects on the properties of the lignin particles.

ScH_2O, while effectively acting as a polar organic solvent to solubilize low molecule weight units within the lignin macromolecule, is ineffective at solubilizing higher molecular weight lignin units. These insoluble units function as sites for undesirable heterogeneous nucleation and aggregation of solubilized lignin species, upon SAS mixing. As such, a small volume of solvent was added to the scH_2O system, to ensure complete solubilization in the high-pressure reactor, and ensure homogenous nucleation upon mixing. Acetone, an easily recyclable organic solvent, is sufficient to serve this purpose, at much lower volumes compared with existing methods for solvent-based synthesis of LNPs. Having a relative permittivity of 20.7 at 25 °C, acetone/water mixtures will have a reduced ε_r compared to pure water systems. It is important to note that no known hazardous reaction exists between acetone and water,[41] and while acetone/water systems have been assessed for changes in their flammability hazard at elevated conditions, acetone concentrations below 25% and 150 °C were assessed as having an explosion class rating of St-0 (no explosion).[42] Several different concentrations of acetone (2.5%, 5%, and 10% v/v) were evaluated for their effectiveness at producing morphologically and chemically uniform and thermally stable LNPs.

Particle morphology analysis with SEM

SEM was performed on the dried scH_2O lignin samples to elucidate the morphology of the lignin particle structure (Fig. 3). Without any acetone to improve solubility and prevent agglomeration during cooling, lignin aggregates inside the reactor vessel and upon quenching. Nanoparticles that do form are aggregated within micrometer-scale particle clumps. A portion of lignin may remain insoluble at the tested subcritical conditions. While subcritical and supercritical water have previously been found to effectively solubilize lignin, prior studies have utilized harsher conditions in order to initiate fractionation and depolymerization of the organic polymer.[21–24] The conditions tested in this work, chosen to reduce thermal degradation of the kraft lignin, may not fully solubilize the lignin, and larger particles may serve as nucleation sites upon SAS mixing, which would explain the clumping of particles evident in SEM of the 0%A lignin sample. Upon the addition of acetone, the formation of uniform nanoparticles is evident. As the percentage of acetone increases from 2.5% up to 10% of the total sample volume, average particle size decreases, while span decreases most significantly for 10%A LNP. Importantly, all three acetone-containing samples demonstrate synthesis of spherical nanoparticles, with few irregular or elongated shapes present for the 10%A LNP sample. Previous research has demonstrated the efficacy of acetone/water cosolvent mixtures to produce LNPs, though these works utilize a much higher volume of acetone (*i.e.*, 70% acetone, 30% water) for the effective synthesis of nanoparticles.[43] Fig. 4 shows selected studies that have utilized solvents for LNP synthesis, and calculated solvent volumes required for treatment of 1 gram of lignin for nanoparticle production.[31,35,43–58] At a concentration of 5 g L^{-1}, sample 10%A LNP uses 20 mL of acetone per treatment of 1 gram of kraft lignin, while comparable studies rely on volumes several times greater.

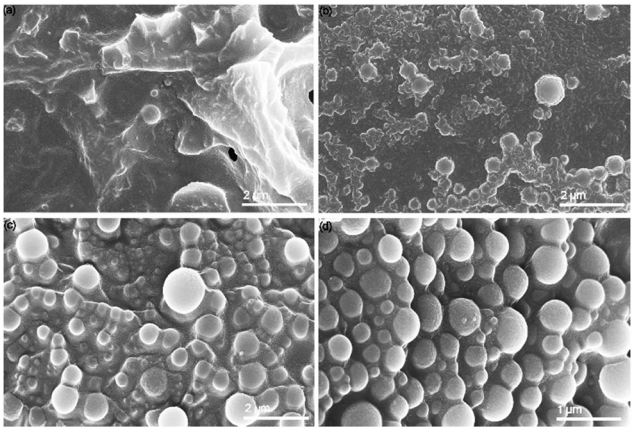

Fig. 3 SEM images of (a) 0%A lignin, showing non-uniform, irregular structure (b) 2.5%A LNPs, showing partial nucleation of nanoparticles (c) 5%A LNPs showing increased volume of nanoparticles (d) 10%A LNPs, showing further increased volume of nanoparticles.

Fig. 5 shows sample 10%A LNP with higher dilution to better clarify the morphology of the synthesized nanoparticles, revealing no amorphous regions or non-spherical structures in this sample. This further demonstrates the enhanced uniformity that the self-assembly process imbues on the particles. Lignin self-assembles into

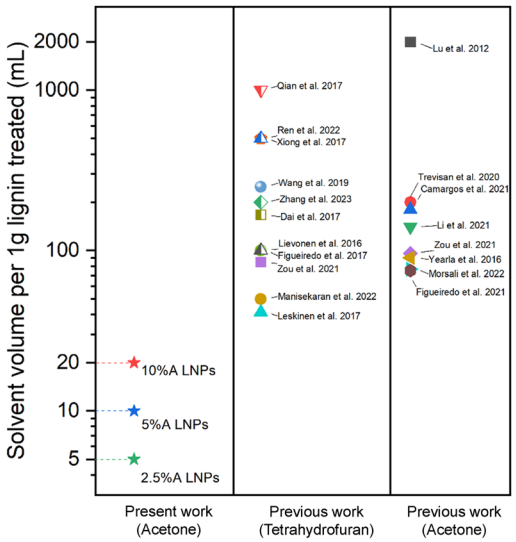

Fig. 4 Selected comparison of solvent volumes required for production of LNPs in prior research utilizing SAS precipitation technique with a variety of solvents.[31,35,43–58] Tetrahydrofuran and acetone are compared, being the two most used solvents for SAS precipitation of LNPs. For studies that used a range of lignin-in-solvent concentrations, the highest concentrations (least volume of solvent used) were shown here.

spheres by molecular rearrangement, with initial nucleation driven by π–π stacking interactions between the hydrophobic aromatic rings.[59] These high molecular weight structures form the interior core of the nuclei. Lower molecular-weight and more hydrophilic units in the form of primarily methoxyl, carboxyl, and hydroxyl groups absorb onto the surface of the nuclei.[58,60] These ionized surface groups, especially ionized carboxylic acid groups, provide electrostatic stability in solution, and prevent aggregation.[61] The presence of charged functional groups on the surface of each spherical nanoparticle, evidenced by increasingly negative zeta potential correlated with smaller mean particle diameter (Table 1), can improve theoretical yield of functionalized lignin products, as these processes rely on chemical interactions with the functional groups of lignin rather than the stable aromatic ring structures of the molecule.[62] Formation of spherical shapes, rather than other nonuniform structures (*i.e.*, rough edges or elongated structures), is due to the understood affinity for molecular nucleation to favor minimization of surface energy by minimizing surface area to volume ratio, resulting in a perfect sphere shape being preferred during particle formation.

Laser diffraction particle size analysis

To investigate the particle size distribution of produced samples, laser diffraction analysis was used, to gain a better understanding of the polydispersity of samples. Particles below 10 nm in diameter cannot be reliably measured with laser diffraction analysis, though this method of analysis provides a more comprehensive picture of sample makeup compared with dynamic light scattering (DLS).[63] DLS performs well with relatively monodisperse nanoparticle samples, but poorly with more polydisperse samples. Laser diffraction analysis gives a more complete picture of the partially or totally homogenous nucleation of LNPs and allows us to use span values as a measure of the breadth of particle diameter distribution (Table 1). Fig. 6a shows that 0%A lignin samples had a negligible volume of particles below 1000 nanometers, and a similar volume density of micrometer-sized particles as untreated kraft lignin dispersed in water, which may be due to in-reactor aggregation of the lignin. Acetone in increasing concentrations showed increasing volumes of nanoparticles, and conversely, a decreasing volume of particles above 1000 nanometers. Higher volumes of acetone increase the dissolution of all

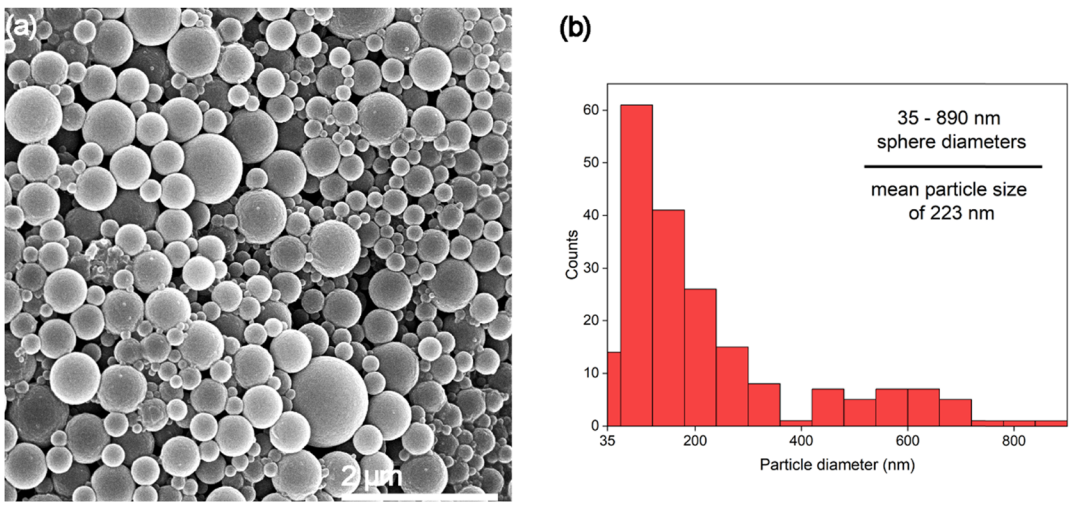

Fig. 5 (a) SEM image of highly diluted (0.01 wt%) 10%A LNPs, showing high yield of spherical nanoparticles without evidence of aggregation or irregular shape formation (b) particle size histogram (calculated using ImageJ analysis software), of image Fig. 5a.

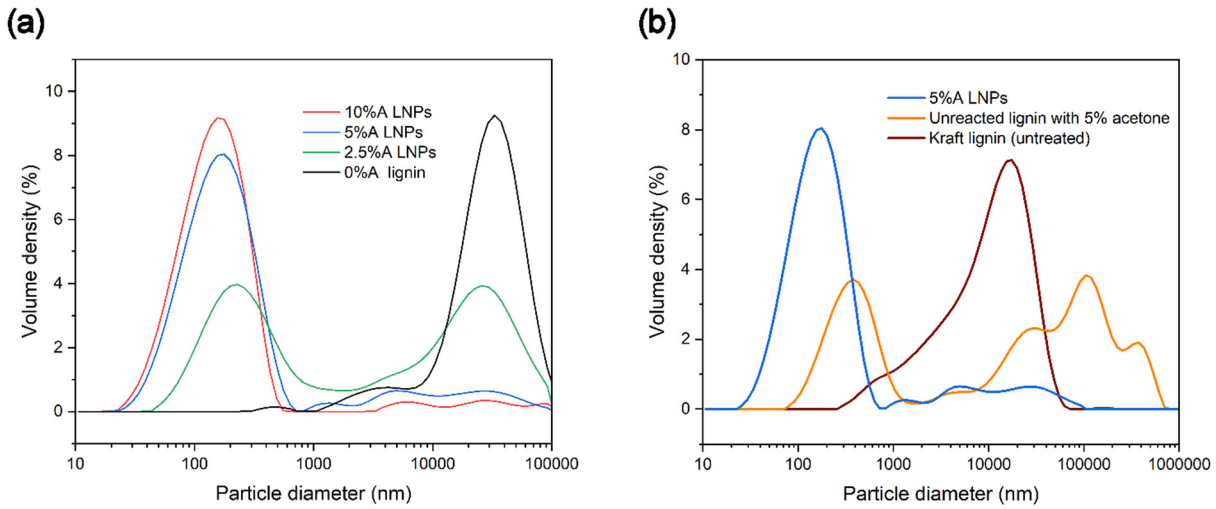

Fig. 6 (a) Particle size distribution graph of lignin particle and nanoparticle suspensions, showing a correlation between increasing acetone concentration and decreasing mean particle size. (b) Comparison of an untreated 5%A LNP sample with a scH_2O-treated samples, demonstrating increased yield when treated.

lignin compounds in the scH_2O/acetone mixtures, which reduces the chance of heterogeneous nucleation sites existing in the form of insoluble lignin particles. While the highest volume of nanoparticles was identified as sample 10%A LNPs (maximum volume density at 156 nm), sample 5%A LNPs achieved a slightly lower volume of nanoparticles (maximum volume density at 177 nm).

Additionally, a sample identical to 5%A LNP, excluding treatment at subcritical conditions or SAS precipitation, was tested to clarify the importance of the novel addition of subcritical treatment for high-yield nanoparticle production (Fig. 6b). Importantly, the LNP sample produced through the novel scH_2O synthesis method had a higher volume of nanoparticles compared with purely acetone/water mixtures without scH_2O treatment (labeled as "unreacted lignin with 5% acetone").

Thermal treatment from scH_2O

Thermal stability and rate of thermal decomposition were analyzed by use of TGA under a nitrogen atmosphere. Similarly with chemical composition changes, decreased thermal stability was evident for samples that were treated at elevated temperatures above 150 °C. Samples that were produced through the studied conditions of 100 °C and 20 MPa, with a 1-hour residence time at these conditions,

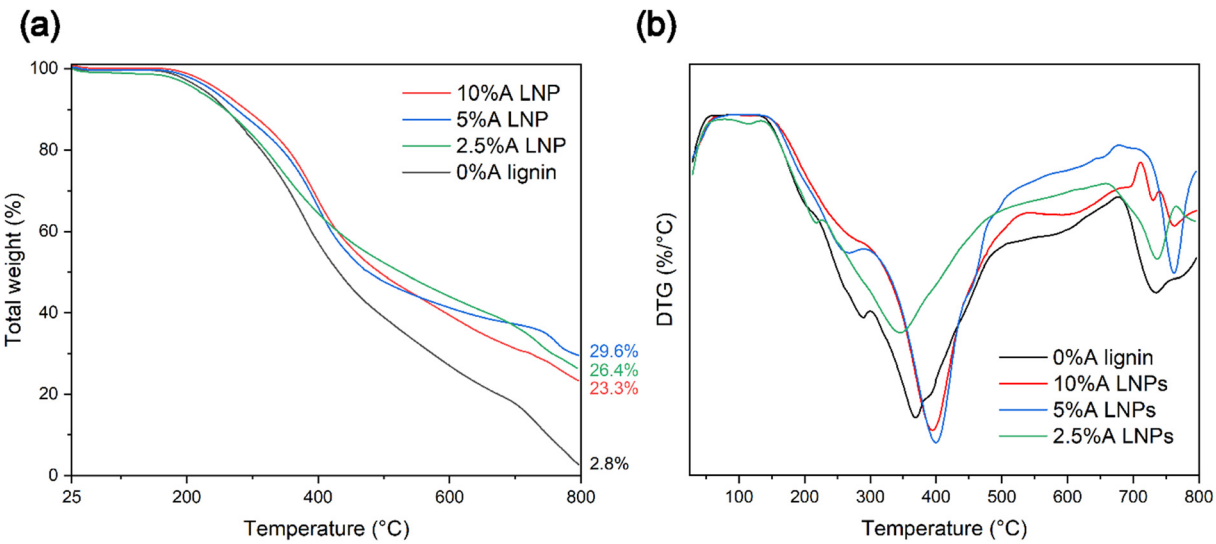

Fig. 7 (a) TGA curves of oven-dried lignin samples, under nitrogen atmosphere, with ramp rates of 10 °C per minute, up to 800 °C, showing improved thermal stability for LNP samples, and (b) DTG graphs representing rate of mass loss per heating rate for oven-dried lignin samples, showing thermal degradation steps consist with unmodified kraft lignin.

displayed varying thermal degradation characteristics correlated with the particle size of the resultant lignin material. Thermogravimetry curve analysis for all synthesized LNP samples revealed expected degradation steps, consistent with that of untreated kraft lignin (Fig. 7a).[64] These samples followed the expected degradation steps of softwood lignin, with three distinctive steps of thermal degradation.[65] The initial step, occurring from temperatures near 120 °C up to 250–275 °C, represents removal of trace moisture bound in the lignin molecule, followed by dehydration of hydroxyl group side chains of the lignin. The second step, representing the step with the most rapid rate of degradation, occurs from approximately 250 °C to 500 °C. In this temperature range, functional side groups, including carbonyl, carboxyl, methoxyl, and sulfonic acid groups, are separated and eliminated through oxidative reactions. The third step, above 500 °C, represents decomposition through cleavage of the remaining aromatic ring clusters, followed by eventual carbonization.

Samples 2.5%A LNP, 5%A LNP and 10%A LNP, which produced nanoparticles after synthesis, demonstrated thermal stability equivalent to that of unmodified kraft lignin, with temperatures (T_{onset}) of 282.9 °C and 291.5 °C, for 5%A LNPs and 10%A LNPs, respectively. Thermal stability of processed kraft LNPs, compared with raw kraft lignin, is consistent with previous literature,[66,67] as well as for LNP-composites,[68] which may be due to higher amounts of phenolic hydroxyl groups. Heat treatment of lignin, which leads to condensation of the lignin macromolecule, and crosslinking of phenolic hydroxyl groups, can also improve the thermal stability of lignin.[69,70] However, higher temperatures than the conditions of this study may be necessary to initiate this crosslinking,[71] providing an intriguing avenue for further research.

Additionally, the high volume of π–π stacking interactions between higher molecular-weight aromatic ring units has been shown to increase thermal stability of polymers by limiting molecular mobility.[72] These interactions are not present in such high density in samples that failed to either entirely or partially self-assemble into nanoparticles upon SAS mixing (samples 0%A lignin and 2.5%A LNP), and these samples had more rapid onset of thermal degradation (Fig. 7b). Sample 2.5%A LNP, having partial nanoparticle self-assembly, but retaining a more amorphous structure compared with samples 5%A LNP and 10%A LNP, did demonstrate similar thermal decomposition (after T_{onset}, from a weight fraction standpoint) to those samples, showing that in-reactor thermal decomposition was reduced for all acetone-assisted samples. The low ash content of 0%A lignin compared with other samples is due to the scH_2O-insoluble, high M_w aromatic groups in lignin that agglomerated onto the interior of the reactor vessel during treatment, contributing to the lower yield of this sample (71%). Given that the majority of this lost mass was most likely more thermally-stable aromatic rings, this caused sample 0%A lignin to have reduced thermal stability compared with other samples when analysed by TGA.

Sample properties

Lignin sample yield increased with higher acetone concentration, due to lower amounts of aggregates sticking to the interior body of the reactor vessel. While the true yield of nanoparticles is difficult to accurately assess, based on SEM imagery, 10%A LNP samples were comprised almost entirely of particles below 900 nm in size, with mean particle sizes of 223 nm, and likely had decreasing yield of microparticles with increasing acetone concentrations, evidenced by laser diffraction particle size analysis. High sample yield is especially important for considering LNP usage in high-value applications that seek to replace existing, high-yield manufacturing of polymers or fillers with LNPs.

Suspension stability and solubility

Fig. 8 shows photographs taken of the produced lignin and LNPs in solution at 1 wt% concentration, after 5 minutes of sonication. In contrast with the acetone-free sample (0%A lignin), which demonstrated rapid settling over a period of just 15 minutes, all acetone-containing samples demonstrated minimal settling over a period of 24 hours. The increased particle–particle repulsion caused by the rearrangement of less-hydrophilic carboxylic acid groups on the exterior of the particle causes repulsive forces that resist settling and imbue the LNP solution with colloidal stability in water.[44,61] Additionally, Hansen solubility parameters (HSPs) for unmodified kraft lignin and our 10%A LNP sample were determined (Fig. S5†). Kraft lignin was found to have HSPs of δD: 17.6, δP: 13.7, δH: 18.1, and R_O of 17, while 10%A LNPs were found to have HSPs of δD: 17, δP: 13.4, δH: 16.5, and R_O of 20.75. Essentially, out of 20 common solvents tested, both samples were found to be fully soluble in only dimethyl sulfoxide, ethylene glycol, *N*,*N*-dimethyl acetamide, and *N*,*N*-dimethyl formamide, while 10%A LNP was found to additionally be fully soluble in acetone, as would be expected. Partial solubility in 1,4-dioxane, ethanol, methanol, ethyl acetate, and tetrahydrofuran remained unchanged between unmodified kraft lignin and 10%A LNPs. These results indicate that while LNPs may have improved colloidal stability in water systems, their solubility in organic solvents is not greatly altered by this treatment process.

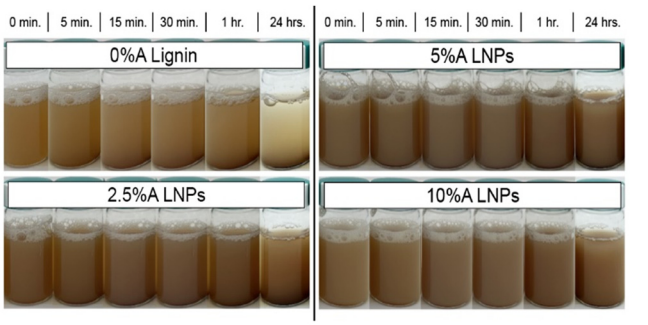

Fig. 8 Images of sample settling over time. All samples demonstrated improved stability compared with 0%A lignin, with 10%A LNPs showing the least settling over 24 hours.

Conclusions

Uniform, spherical LNPs were synthesized by a novel process, using subcritical H_2O and low volumes of organic solvent. The SAS approach was successfully replicated by using a subcritical H_2O solution with recyclable acetone as the solvent phase for kraft lignin, and an ice water bath as the antisolvent phase. The produced nanoparticles at a concentration of 10% acetone showed minimal aggregation, with individualized, well-defined lignin spheres (diameter, $d < 1000$ nm). Importantly, acetone-assisted nanoparticle samples showed smaller mean particle size, higher end-product yield, improved suspension stability in water, and higher thermal stability, compared with pure-scH_2O samples (0%A lignin). The proposed organic solvent lean system can be considered a more sustainable (*vs.* traditional SAS approach), and efficient method to produce a renewable, bio-based material in the form of LNPs. Such a chemically and morphologically uniform lignin nanomaterials have potential use in a wide range of high-value applications, including Pickering emulsion stabilization, polymer additives, and functionalized lignin products.

Author contributions

E. J. F.: conceptualization, resources, writing – review & editing, supervision, and funding acquisition. P. S. M.: methodology, formal analysis, investigation, data curation, writing – original draft preparation. M. H.: methodology, writing – review and editing. F. B. S.: investigation, writing – review and editing. V. F.: investigation, writing – review and editing.

Conflicts of interest

There are no conflicts to declare.

Acknowledgements

The authors gratefully acknowledge the financial support provided by the NSERC Canfor Industrial Research Chair in Advanced Bioproducts, (# 553449 - 19), NSERC Discovery Grant (RGPIN-2021-03172), the Canada Foundation for Innovation (Project number 022176) and Pacific Economic Development Canada (PacifiCan). UBC Centre for High-Throughput Phenogenomics is acknowledged for providing SEM imaging facilities. R. Osei-Bonsu is gratefully acknowledged for AFM imaging.

Notes and references

1 N. R. Maddela, B. Ramakrishnan, D. Kakarla, K. Venkateswarlu and M. Megharaj, *RSC Adv.*, 2022, **12**, 12396–12415.
2 L. A. Zevallos Torres, A. Lorenci Woiciechowski, V. O. de Andrade Tanobe, S. G. Karp, L. C. Guimarães Lorenci, C. Faulds and C. R. Soccol, *J. Cleaner Prod.*, 2020, **263**, 121499.
3 T. D. H. Bugg, J. J. Williamson and G. M. M. Rashid, *Curr. Opin. Chem. Biol.*, 2020, **55**, 26–33.
4 P. Bajpai, *Biermann's handbook of pulp and paper: raw material and pulp making*, Elsevier, Amsterdam, Netherlands, Cambridge, MA, 3rd edn, 2018.
5 G. A. Smook, *Handbook for pulp & paper technologists*, Tappi Press, Peachtree Corners, GA, 4th edn, 2016.
6 A. Boarino and H.-A. Klok, *Biomacromolecules*, 2023, **24**, 1065–1077.
7 Y. Zhang and M. Naebe, *ACS Sustainable Chem. Eng.*, 2021, **9**, 1427–1442.
8 X. Lu, X. Gu and Y. Shi, *Int. J. Biol. Macromol.*, 2022, **210**, 716–741.
9 L. E. Low, K. C. Teh, S. P. Siva, I. M. L. Chew, W. W. Mwangi, C. L. Chew, B.-H. Goh, E. S. Chan and B. T. Tey, *Environ. Nanotechnol., Monit. Manage.*, 2021, **15**, 100398.
10 Y. Qian, Q. Zhang, X. Qiu and S. Zhu, *Green Chem.*, 2014, **16**, 4963–4968.
11 Y. Qian, X. Qiu, X. Zhong, D. Zhang, Y. Deng, D. Yang and S. Zhu, *Ind. Eng. Chem. Res.*, 2015, **54**, 12025–12030.
12 M. S. Alqahtani, A. Alqahtani, A. Al-Thabit, M. Roni and R. Syed, *J. Mater. Chem. B*, 2019, **7**, 4461–4473.
13 T. Zou, M. H. Sipponen, A. Henn and M. Österberg, *ACS Nano*, 2021, **15**, 4811–4823.
14 B. Zhao, M. Borghei, T. Zou, L. Wang, L.-S. Johansson, J. Majoinen, M. H. Sipponen, M. Österberg, B. D. Mattos and O. J. Rojas, *ACS Nano*, 2021, **15**, 6774–6786.
15 J. Wang, W. Chen, D. Yang, Z. Fang, W. Liu, T. Xiang and X. Qiu, *ACS Nano*, 2022, **16**, 20705–20713.
16 S. Beisl, A. Miltner and A. Friedl, *Int. J. Mol. Sci.*, 2017, **18**, 1244.
17 S. Iravani and R. S. Varma, *Green Chem.*, 2020, **22**, 612–636.
18 A. Lourenço and J. Gominho, in *Lignin*, ed. A. Sand and J. Tuteja, IntechOpen, Rijeka, 2023, ch. 7.
19 W. Gao and P. Fatehi, *Can. J. Chem. Eng.*, 2019, **97**, 2827–2842.
20 Y. Pu, J.-X. Wang, D. Wang, N. R. Foster and J.-F. Chen, *Chem. Eng. Process.*, 2019, **140**, 36–42.
21 M. S. Celiktas, M. Yaglikci and F. Khosravi Maleki, *Polym. Test.*, 2019, **77**, 105918.
22 A. Martínez-Abad, N. Giummarella, M. Lawoko and F. Vilaplana, *Green Chem.*, 2018, **20**, 2534–2546.
23 Y. Qian, C. Zuo, J. Tan and J. He, *Energy*, 2007, **32**, 196–202.
24 J. Lappalainen, D. Baudouin, U. Hornung, J. Schuler, K. Melin, S. Bjelić, F. Vogel, J. Konttinen and T. Joronen, *Energies*, 2020, **13**, 3309.
25 F. de Boer, *PhD Thesis*, Utrecht University, 2019.
26 M. Uematsu and E. U. Franck, *J. Phys. Chem. Ref. Data*, 1980, **9**, 1291–1306.
27 B. M. Nolan, E. K. Chan, X. Zhang, E. Muthuswamy, K. van Benthem and S. M. Kauzlarich, *ACS Nano*, 2016, **10**, 5391–5397.
28 M. Meyns, S. Willing, H. Lehmann and C. Klinke, *ACS Nano*, 2015, **9**, 6077–6087.

29 D. Rudolph, N. Redinger, K. Schwarz, F. Li, G. Hädrich, M. Cohrs, L. A. Dailey, U. E. Schaible and C. Feldmann, *ACS Nano*, 2023, **17**, 9478–9486.
30 H. K. Valo, P. H. Laaksonen, L. J. Peltonen, M. B. Linder, J. T. Hirvonen and T. J. Laaksonen, *ACS Nano*, 2010, **4**, 1750–1758.
31 P. Figueiredo, K. Lintinen, A. Kiriazis, V. Hynninen, Z. Liu, T. Bauleth-Ramos, A. Rahikkala, A. Correia, T. Kohout, B. Sarmento, J. Yli-Kauhaluoma, J. Hirvonen, O. Ikkala, M. A. Kostiainen and H. A. Santos, *Biomaterials*, 2017, **121**, 97–108.
32 L. Chen, Y. Shi, B. Gao, Y. Zhao, Y. Jiang, Z. Zha, W. Xue and L. Gong, *ACS Sustainable Chem. Eng.*, 2020, **8**, 714–722.
33 V. Dighe, P. K. R. Podupu, P. Coliaie and M. R. Singh, *Cryst. Growth Des.*, 2022, **22**, 3119–3127.
34 I. Pylypchuk and M. H. Sipponen, *Green Chem.*, 2022, **24**, 8705–8715.
35 A. Manisekaran, P. Grysan, B. Duez, D. F. Schmidt, D. Lenoble and J.-S. Thomann, *J. Colloid Interface Sci.*, 2022, **626**, 178–192.
36 C. Liu, Y. Li and Y. Hou, *Eur. Polym. J.*, 2019, **112**, 15–23.
37 G. Carr, R. Mammucari and N. R. Foster, *Chem. Eng. J.*, 2011, **172**, 1–17.
38 J. Zhang, Z. Tian, X. Ji and F. Zhang, *Polymer*, 2022, **14**, 4196.
39 M.-W. Park and S.-D. Yeo, *Chem. Eng. Res. Des.*, 2012, **90**, 2202–2208.
40 Y. Wang, J. Song, S. F. Chow, A. H. L. Chow and Y. Zheng, *Int. J. Pharm.*, 2015, **494**, 479–489.
41 H. M. Yusoff, L. K. Li, S. Izhar and M. S. Md Said, *Case Stud. Therm. Eng.*, 2021, **28**, 101631.
42 Y. Chang, J. Lee, S. Wu, C.-C. Chen and C. Shu, *J. Therm. Anal. Calorim.*, 2009, **95**, 525–534.
43 X. Li, J. Shen, B. Wang, X. Feng, Z. Mao and X. Sui, *ACS Sustainable Chem. Eng.*, 2021, **9**, 5470–5480.
44 M. Lievonen, J. J. Valle-Delgado, M.-L. Mattinen, E.-L. Hult, K. Lintinen, M. A. Kostiainen, A. Paananen, G. R. Szilvay, H. Setälä and M. Österberg, *Green Chem.*, 2016, **18**, 1416–1422.
45 Q. Lu, M. Zhu, Y. Zu, W. Liu, L. Yang, Y. Zhang, X. Zhao, X. Zhang, X. Zhang and W. Li, *Food Chem.*, 2012, **135**, 63–67.
46 S. R. Yearla and K. Padmasree, *J. Exp. Nanosci.*, 2016, **11**, 289–302.
47 P. Figueiredo, M. H. Lahtinen, M. B. Agustin, D. M. de Carvalho, S.-P. Hirvonen, P. A. Penttilä and K. S. Mikkonen, *ChemSusChem*, 2021, **14**, 4718–4730.
48 C. H. M. Camargos and C. A. Rezende, *Int. J. Biol. Macromol.*, 2021, **193**, 647–660.
49 M. Morsali, A. Moreno, A. Loukovitou, I. Pylypchuk and M. H. Sipponen, *Biomacromolecules*, 2022, **23**, 4597–4606.
50 B. Wang, D. Sun, H.-M. Wang, T.-Q. Yuan and R.-C. Sun, *ACS Sustainable Chem. Eng.*, 2019, **7**, 2658–2666.
51 I. Dai, R. Liu, L.-Q. Hu, Z.-F. Zou and C.-L. Si, *ACS Sustainable Chem. Eng.*, 2017, **5**, 8241–8249.
52 T. Leskinen, M. Smyth, Y. Xiao, K. Lintinen, M.-L. Mattinen, M. A. Kostiainen, P. Oinas and M. Österberg, *Nord. Pulp Pap. Res. J.*, 2017, **32**, 586–596.
53 Y. Qian, X. Zhong, Y. Li and X. Qiu, *Ind. Crops Prod.*, 2017, **101**, 54–60.
54 C. Ren, M. Li, W. Huang, Y. Zhang and J. Huang, *J. Mater. Sci.*, 2022, **57**, 18356–18369.
55 H. Trevisan and C. A. Rezende, *Ind. Crops Prod.*, 2020, **145**, 112105.
56 F. Xiong, Y. Han, S. Wang, G. Li, T. Qin, Y. Chen and F. Chu, *Ind. Crops Prod.*, 2017, **100**, 146–152.
57 J. Zhang, Z. Tian, X.-X. Ji and F. Zhang, *Int. J. Biol. Macromol.*, 2023, **231**, 123244.
58 T. Zou, N. Nonappa, M. Khavani, M. Vuorte, P. Penttilä, A. Zitting, J. J. Valle-Delgado, A. M. Elert, D. Silbernagl, M. Balakshin, M. Sammalkorpi and M. Österberg, *J. Phys. Chem. B*, 2021, **125**, 12315–12328.
59 I. V. Pylypchuk, P. A. Lindén, M. E. Lindström and O. Sevastyanova, *ACS Sustainable Chem. Eng.*, 2020, **8**, 13805–13812.
60 M. E. Jawerth, C. J. Brett, C. Terrier, P. T. Larsson, M. Lawoko, S. V. Roth, S. Lundmark and M. Johansson, *ACS Appl. Polym. Mater.*, 2020, **2**, 668–676.
61 A. Moreno, J. Liu, R. Gueret, S. E. Hadi, L. Bergström, A. Slabon and M. H. Sipponen, *Angew. Chem., Int. Ed.*, 2021, **60**, 20897–20905.
62 A. Moreno, J. Liu, M. Morsali and M. H. Sipponen, in *Micro and Nanolignin in Aqueous Dispersions and Polymers*, ed. D. Puglia, C. Santulli and F. Sarasini, Elsevier, 2022, pp. 385–431.
63 P. Bowen, *J. Dispersion Sci. Technol.*, 2002, **23**, 631–662.
64 S. Kubo and J. F. Kadla, *J. Wood Chem. Technol.*, 2008, **28**, 106–121.
65 M. Poletto, *Maderas: Cienc. Tecnol.*, 2017, **19**, 63–74.
66 Z. Zhang, C. Belda Marín, M. Lefebvre, C. Lefebvre, V. Terrasson and E. Guénin, *Int. J. Biol. Macromol.*, 2022, **222**, 1830–1839.
67 A. Myint, H. W. Lee, B. Seo, W.-S. Son, J. Yoon, T. J. Yoon, H. J. Park, J. Yu, J. Yoon and Y.-W. Lee, *Green Chem.*, 2016, **18**, 2129–2146.
68 S. Nair, S. Sharma, Y. Pu, Q. Sun, S. Pan, J. Y. Zhu, Y. Deng and A. Ragauskas, *ChemSusChem*, 2014, **7**, 3513–3520.
69 J.-Y. Kim, E.-J. Shin, I.-Y. Eom, K. Won, Y. H. Kim, D. Choi, I.-G. Choi and J. W. Choi, *Bioresour. Technol.*, 2011, **102**, 9020–9025.
70 S. Sen, S. Patil and D. S. Argyropoulos, *Green Chem.*, 2015, **17**, 4862–4887.
71 J.-Y. Kim, H. Hwang, S. Oh, Y.-S. Kim, U.-J. Kim and J. W. Choi, *Int. J. Biol. Macromol.*, 2014, **66**, 57–65.
72 Y. Shi, M. J. van Steenbergen, E. A. Teunissen, L. Novo, S. Gradmann, M. Baldus, C. F. van Nostrum and W. E. Hennink, *Biomacromolecules*, 2013, **14**, 1826–1837.